

Photoreceptor progenitor dynamics in the zebrafish embryo retina and its modulation by primary cilia and N-cadherin

GONZALO APARICIO^{#,1,2}, MAGELA RODAO^{#,1,2}, JOSÉ L. BADANO² and FLAVIO R. ZOLESSI^{*,1,2}

¹Sección Biología Celular, Facultad de Ciencias, Universidad de la República and
²Institut Pasteur Montevideo, Uruguay

ABSTRACT Photoreceptor cells of the vertebrate neural retina originate in the neuroepithelium, and like other neurons, must undergo cell body translocation and polarity transitions to acquire their final functional morphology, which includes features of neuronal and epithelial cells. We analyzed this process in detail in zebrafish embryos using *in vivo* confocal microscopy and electron microscopy. Photoreceptor progenitors were labeled by the transgenic expression of enhanced green fluorescent protein under the regulation of the photoreceptor-specific promoter *crx*, and structures of interest were disrupted using morpholino oligomers to knock-down specific genes. Photoreceptor progenitors detached from the basal retina at pre-mitotic stages, rapidly retracting a short basal process as the cell body translocated apically. They remained at an apical position indefinitely to form the outer nuclear layer (ONL), initially extending and retracting highly dynamic neurite-like processes, tangential to the apical surface. Many photoreceptor progenitors presented a short apical primary cilium. The number and length of these cilia was gradually reduced until nearly disappearing around 60 hpf. Their disruption by knocking-down *ift88* and *elipsa* caused a notorious defect on basal process retraction. To assess the role of cell adhesion in the organization of photoreceptor progenitors, we knocked-down *cdh2*/N-cadherin and observed the cell behavior by time-lapse microscopy. The ectopic photoreceptor progenitors initially migrated in an apparent random manner, profusely extending cell processes, until they encountered other cells to establish cell rosettes in which they stayed, acquiring photoreceptor-like polarity. Altogether, our observations indicate a complex regulation of photoreceptor progenitor dynamics to form the retinal ONL, previous to the post-mitotic maturation stages.

KEY WORDS: *neuroepithelium, cell polarity, cell adhesion, retina lamination, neurogenesis*

Introduction

The central nervous system of vertebrates is originated from a polarized, pseudostratified epithelium, which among other features presents a Laminin1-enriched basal lamina, sub-apical N-cadherin-based adherens junctions and apical primary cilia (Zolessi, 2016). These neuroepithelial cells are the progenitors for both glial cells and neurons. It is hence natural to assume that the epithelial polarized surroundings must influence how neurons acquire their own polarity, and, particularly, orientation inside the tissue. The identity of these signals and their interactions with the early post-mitotic neurons are, however, still poorly understood. The neural retina is a highly approachable region of the central nervous system, ideal for *in vivo* studies of neural differentiation

(Amini *et al.*, 2018). In spite of its relative simplicity, it contains a diversity of cell types, ranging from the very “canonical” neurons such as retinal ganglion cells (RGCs; with a single axon, and opposite branching dendrites), to neurons that partly remain as epithelial cells, like the photoreceptor cells (Hoon *et al.*, 2014). Mutant analyses in zebrafish embryos have indicated that the histogenesis of the retina appears particularly sensitive to the disruption of molecules involved in epithelial cell polarity. Most of the affected genes in these mutants encode for proteins related to apical identity and sub-apical adhesion in epithelial cells, such

Abbreviations used in this paper: aPKC, atypical protein kinase C; Crx, cone-rod homeobox transcription factor; hpf, hours post-fertilization; ONL, outer nuclear layer; RGC, retinal ganglion cell; TEM, transmission electron microscopy.

*Address correspondence to: Flavio R. Zolessi. Sección Biología Celular, Facultad de Ciencias, Universidad de la República, Calle Iguá 4225, Montevideo 11400, Uruguay. Tel: +59825258618, ext. 7144; E-mail: fzolessi@fcien.edu.uy -  <https://orcid.org/0000-0003-2405-994X> - #Note: Equal author contribution

Supplementary Material (2 figures and 15 videos) for this paper is available at: <https://doi.org/10.1387/ijdb.200113fz>

Submitted: 13 February, 2020; Accepted: 11 May, 2020; Published online: 25 August, 2020.

as N-cadherin (mutants known as *parachute*, *glass onion* or *lyra*), Pals1/Mpp5 (*nagie oko*), aPKC λ (*heart and soul*) and Crb2a (*oko meduzy*) (Pujic and Malicki, 2004).

Differentiated photoreceptor cells, cones and rods, are unique cells in many respects. First, the largest part of their cytoplasm and membrane protrudes from the apical side of the cell, beyond the adhesion belt that holds them together with the apical tips of Müller glia (the “outer limiting membrane”). This apical portion consists of the inner segment, highly enriched in membrane organelles and mitochondria, and the outer segment, where a thick stack of membranes contains the photo-transduction machinery. Interestingly, the outer segment is originated from and remains attached to the inner segment through a connecting cilium, essential for the transport of proteins and membrane (Malicki, 2012). The photoreceptor cell body and nucleus are mostly located below the outer limiting membrane, and basally the cell ends in a specialized pre-synaptic terminal, connecting with bipolar and horizontal cells. Alterations in the maintenance of this particular cell polarity, as happens when genes encoding proteins involved in apical adhesions or cilia transport are mutated, can eventually cause retinal degeneration in animals and humans. For example, mutations in Crb genes cause hereditary forms of Leber congenital amaurosis and retinitis pigmentosa (Quinn *et al.*, 2017), while a common symptom in ciliopathies is retinal dystrophy (Whewey *et al.*, 2014). Studying how photoreceptor cells differentiate *in vivo*, particularly at earlier developmental stages when the first polarized signals act on progenitors and early post-mitotic cells, is of vital importance for understanding how these diseases eventually arise.

By *in vivo* imaging, it was shown that photoreceptor cells arise from terminal cell divisions of apically-localized progenitors that already display an epithelial-like conformation, reminiscent of the organization at the mature outer nuclear layer, indicating that polarity constraints are acting very early on the photoreceptor cell lineage (Suzuki *et al.*, 2013; Weber *et al.*, 2014). This process appears to be severely affected in all polarity mutants described above. For example, in *nagie oko* mutant retinas it was shown that photoreceptor cells have a scattered distribution, while in different N-cadherin mutants they tend to form rosettes inside the retina (Masai *et al.*, 2003; Wei *et al.*, 2006). This effect, as it was shown for similar mutants, was non-cell autonomous, indicating the importance of cell-to-cell interactions and adherens junctions during the formation of the outer nuclear layer (ONL; Wei *et al.*, 2006; Zou *et al.*, 2008). In this work, we provide a detailed description of the normal dynamics at early stages of photoreceptor cell differentiation, starting at progenitor stages, as labeled by using fluorescent reporters under the regulation of the *crx* promoter region. In addition, we described for the first time the presence, ultra-structure and localization of primary cilia in these precursor cells, well before the onset of outer segment formation. These observations set us to explore the functions of primary cilia and cadherin-based adhesion in early photoreceptor differentiation. The knock-down of relevant genes involved in the maintenance of these structures (*cdh2* for cell adhesion; *ift88* and *elipsa* for cilia) using previously reported, well-characterized morpholino oligomers (Lele *et al.*, 2002; Lepanto, Davison, *et al.*, 2016), indicated they play different roles on photoreceptor precursor organization in the intact zebrafish retina.

Results

Dynamic behavior of photoreceptor progenitors during the establishment of the outer nuclear layer (ONL)

We labeled photoreceptor cells using the regulatory region of the cone-rod homeobox gene (*crx*) to drive the expression of membrane-directed EGFP-CAAX (*crx*:GFP), a construct that is expressed from progenitor stages (Suzuki *et al.*, 2013). Similar to what has been previously shown (Weber *et al.*, 2014), we observed here a gradual formation of the ONL, between approximately 36 and 60 hpf (Fig. 1A). This is evidenced by transmission electron microscopy (TEM) as well (Fig. 1B), where we could detect photoreceptor progenitors at early stages like 36 hpf by crossing *crx*:GFP transgenic with APEX-GBP transgenic lines (Ariotti *et al.*, 2015). At 48 hpf, the photoreceptor progenitors already formed a highly ordered sheet of cells at the apical side of the retina, while cell divisions were still evident (Fig 1). The epithelial-like organization of the ONL at 48 and 60 hpf was confirmed by immunolabeling with anti-pan-cadherin and anti-aPKC ζ antibodies, showing an apical accumulation of both molecular markers at these stages on *crx*:GFP-expressing cells (Fig. 1 D,E). Interestingly, F-actin was accumulated at a thinner apical region in these cells at 48 than at 60 hpf, with a proportionally higher coincidence with cadherins at the later stage (Fig. 1D). At 48 hpf, most of the cadherin signal was excluded from the thinner apical F-actin-rich zone. In the case of the apical marker aPKC ζ , however, signal was always restricted to the apical-most aspect of *crx*:GFP cells, not coinciding with the basal-most F-actin accumulation where pan-cadherin signal was evident at 60 hpf (Fig. 1E).

Time-lapse confocal microscopy of *crx*:GFP-expressing cells (from 36 hpf) showed a progressive signal increase, with a good detection of photoreceptor progenitors localized around the central area of the retinal neuroepithelium, from where they translocated their nuclei apically (Fig. 2 A,C and Supplementary Video 1). As undergoing this apical movement, some photoreceptor progenitors presented a short basal process, while others just had a smooth basal side (Fig. 1A and 2 A-C). In a few occasions, very dimly fluorescent *crx*:GFP-positive cells were detected which appeared attached to the retinal basal surface through a very thin process. Fig. 2D and Supplementary Video 2 shows how the basal process in one of these cells is quickly retracted as the nucleus starts to translocate apically. All along the process, the observed cells remained attached to the apical border of the retinal neuroepithelium, initially through an apical process that quickly shortened until it disappeared as the cell body translocated to the future ONL (Fig. 2 A,C and Supplementary Video 1). This phenomenon of nuclear translocation was clearly seen in most *crx*:GFP-expressing cells at 36 hpf, and in cells located around the central patch of differentiating retina at 40 and 48 hpf (also see Fig. 3 and associated Supplementary Videos). A quantification of cell body translocation showed that since clearly detected, photoreceptor progenitors presented a net directional movement towards the apical border of the neuroepithelium, albeit with varying speeds and eventual reversed direction, taking a total time between 2 and 4 hours (Fig. 2E,F). Once translocated to the ONL, photoreceptor progenitors stayed permanently in that apical position, eventually dividing between 5 and 8 h after arriving, without any visible interkinetic nuclear migration (Fig. 2 B,G and Supplementary videos 1 and 3).

During this period, and particularly between 36 and 48 hpf,

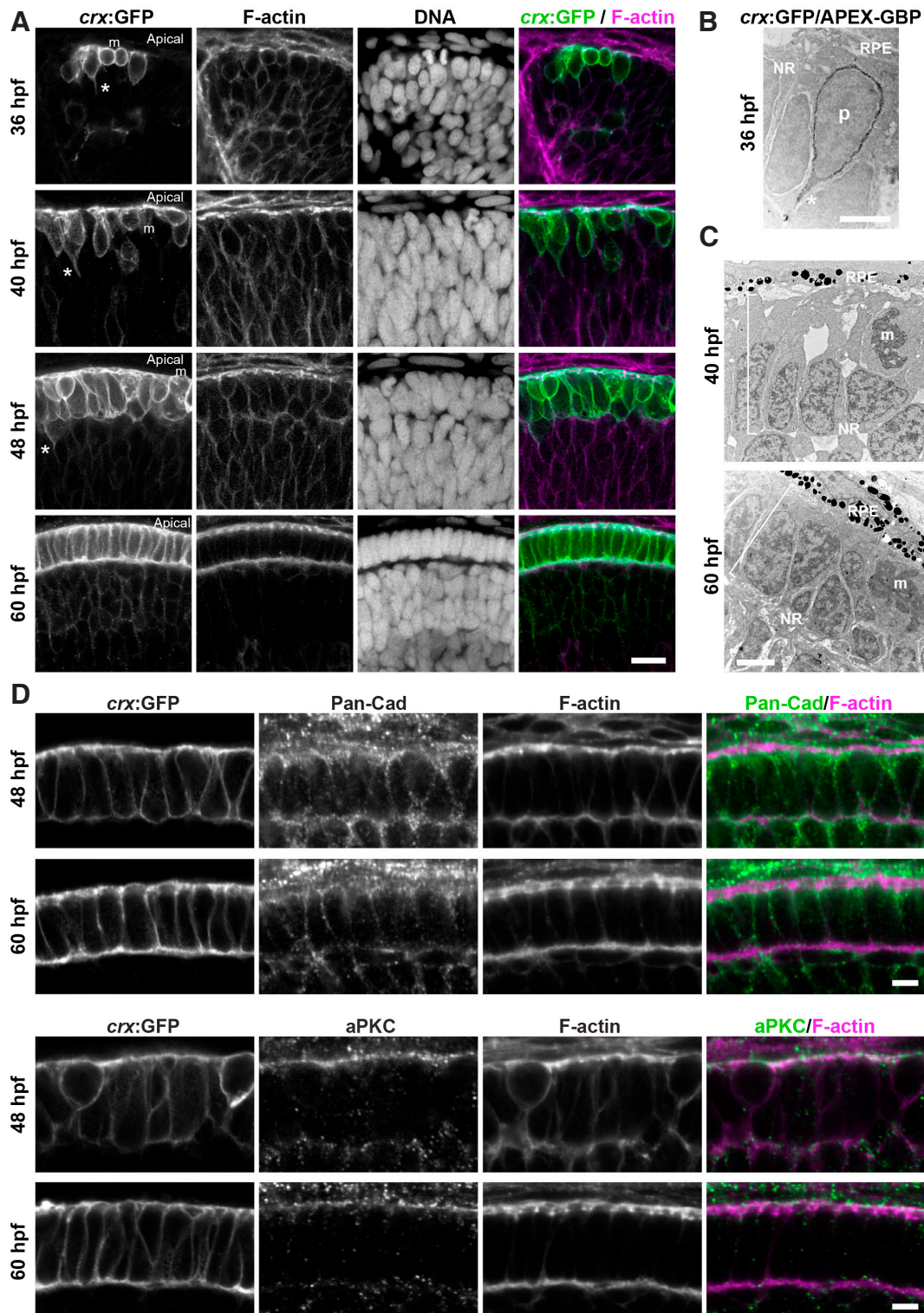


Fig. 1. Formation of the outer nuclear layer in the early stages of retina histogenesis. (A) Series of confocal images from zebrafish embryo retinas at different developmental stages, transgenically labeled with *crx:EGFP-CAAX* (*crx:GFP*). *m*: mitotic cells; asterisks: basal processes. 36 and 60 hpf, single confocal sections; 40 and 48 hpf, maximum intensity projections of four sections, at 0.37 μm separation. **(B)** Transmission electron microscopy (TEM) of *crx:GFP/APEX-GBP* double transgenic embryo at 36 hpf. Binding of the modified peroxidase APEX-GBP to GFP allows for the generation of a DAB precipitate around the cell periphery of photoreceptor progenitors (*p*). NR: neural retina; RPE: retinal pigmentary epithelium; asterisk: basal process. **(C)** TEM of the outer retina at later stages; the ONL (brackets) starts to become evident as photoreceptor progenitors elongate and acquire an epithelial-like conformation. NR: neural retina; RPE: retinal pigmentary epithelium; *m*: cells undergoing mitosis. **(D,E)** High magnification confocal images of the apical region of *crx:GFP*-transgenic embryos labeled with anti-pan-cadherin (D) and anti-aPKC ζ antibodies (E). Scale bars: A, 10 μm ; B-C, 2 μm ; D-E: 5 μm .

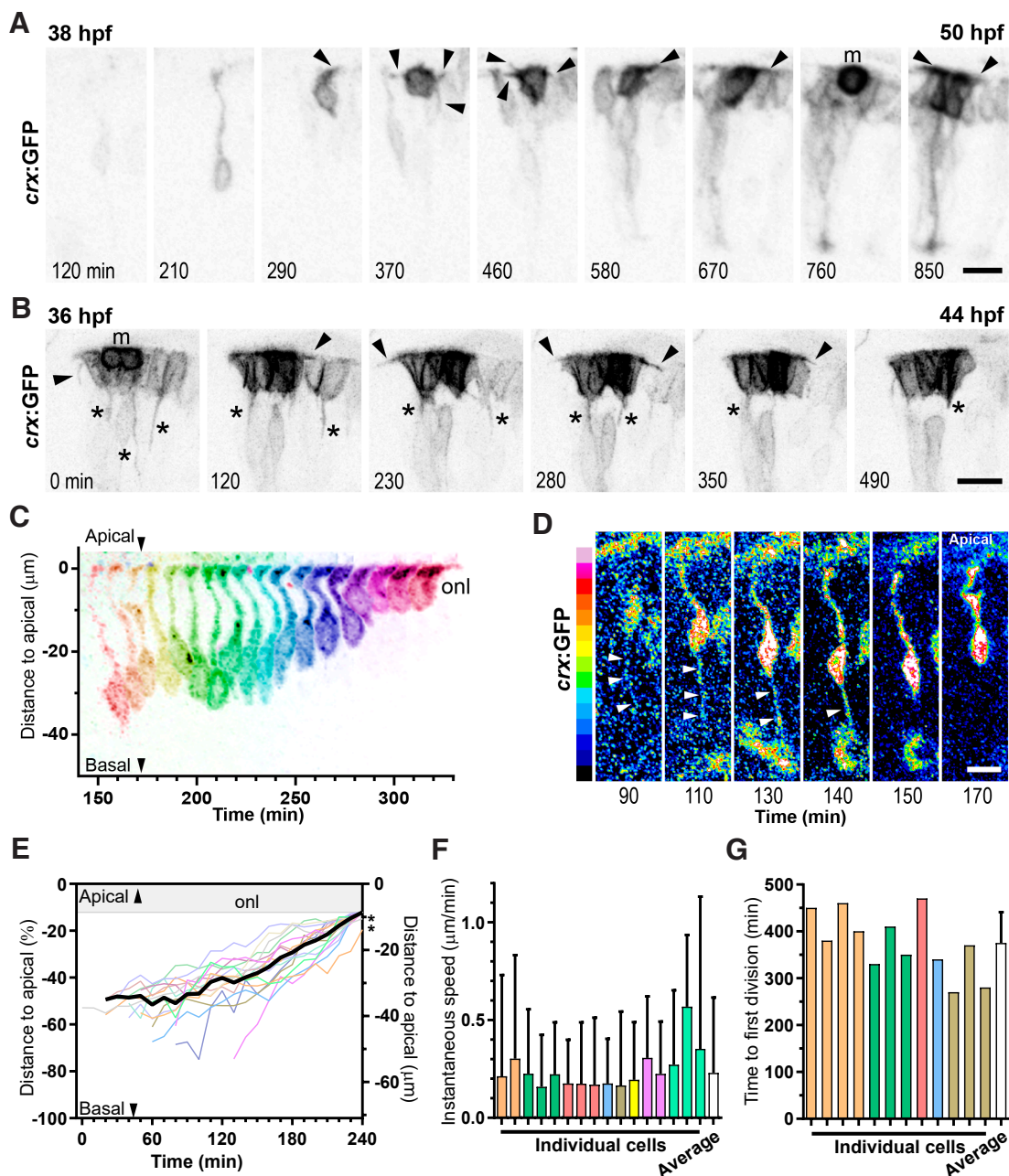


Fig. 2. Dynamics of photoreceptor progenitor translocation to the forming outer nuclear layer. (A,B) Maximum intensity projections from time lapse confocal images of *crx:GFP*-injected retinas, from 36 hpf. The series in (A) shows the initial process until the first cell division is shown: a photoreceptor progenitor starts to be detected at time=120 min, and as the *crx:GFP* signal increases (image brightness was adjusted from 580 min to improve visualization), its cell body translocates to the ONL, undergoing cell division at $t=760$ min (cell marked "m"). See Supplementary Video 1. (B) Shows the dynamics of a group of photoreceptor progenitors, since the moment one of them divides. See Supplementary Video 3. Arrowheads: cell processes from the apical side of the cell; asterisks: basal processes; time in min. (C) Digital superposition of the image of the photoreceptor progenitor observed in A, including all time points (acquired every 10 min) from $t=150$ to 320 min. (D) Observation of the same cell at earlier stages, increasing brightness and converting to a 16-color intensity code, to evidence the presence of a thin basal process (arrowheads) while the cell body translocates basally. Basal detachment and complete retraction of the basal process (white arrowheads) appears to happen between $t=140$ and 150 min, just before the cell starts to move apically. See Supplementary Video 2. (E) Trajectories in time of several *crx:GFP*-positive cell bodies, since they are detected until they reach the ONL ("onl"). The thick black line at the front shows the average trajectories of all cells, excluding two that did not reach the final position at the end of the time lapse (marked with asterisks). Distance from the base of the cell body to the apical surface was measured for every cell, at each time point, and distances normalized to the width of the neuroepithelium ($70.8 \mu\text{m}$, represented on the right y axis). $n=16$ cells, 8 embryos, 3 independent experiments. (F) Averaged instantaneous speeds of nuclear translocation for each cell shown in D. Instantaneous speed was calculated by dividing the displacement in μm between two timepoints, divided by the time between frames (10 min); bars show mean + SD, and colors represent cells from different embryos. The white bar shows the average instantaneous speeds for all cells, and SD ($0.23 \pm 0.39 \mu\text{m}/\text{min}$). (G) Time between apical positioning at the ONL and first cell division of 12 different *crx:GFP*-positive cells (6 embryos; 3 experiments). White bar: mean + SD. Scale bars: $10 \mu\text{m}$.

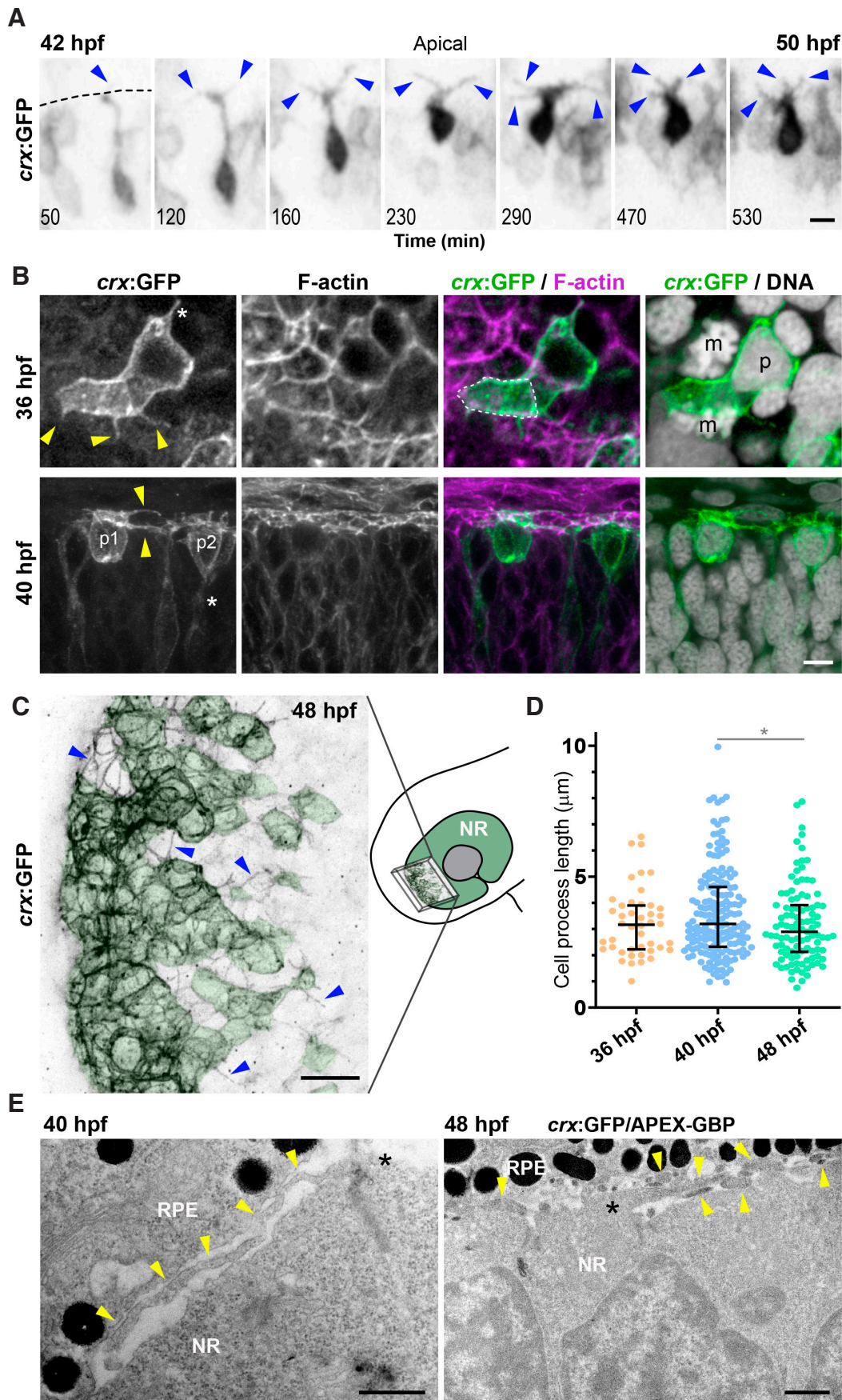


Fig. 3. Photoreceptor progenitors extend dynamic cell processes while forming the outer nuclear layer. (A) Maximum intensity projections from a time lapse confocal image of a *crx:GFP*-injected embryo retina. An isolated photoreceptor progenitor dynamically extends and retracts tangential processes (blue arrowheads) from 42 to 50 hpf. Dashed line: apical region. **(B)** Confocal images of *crx:GFP* transgenic embryos, tangential (36 hpf) and perpendicular (40 hpf) to the apical retina. Yellow arrowheads: tangential processes; asterisks: basal processes; m: mitotic cell; p: photoreceptor progenitor nucleus; white dashed line: apical membrane of a photoreceptor progenitor. Maximum intensity projections of 4 (36 hpf) and 14 (40 hpf) sections, at a $0.37 \mu\text{m}$ separation. See Supplementary Videos 5 and 7. **(C)** Tangential view of a 48 hpf retina, at the periphery of the differentiating nasal-ventral patch (maximum intensity projection of 14 sections, at $0.5 \mu\text{m}$ separation). Blue arrowheads: tangential processes; green shaded area: photoreceptor progenitor cell bodies. The drawing on the right shows the approximate position and angle of the confocal stack. **(D)** Comparative quantification of tangential process length at different stages (median and 25/75% percentile). N: 36 hpf, 44 processes from 9 embryos; 40 hpf, 174 processes, 12 embryos; 48 hpf, 103 processes, 9 embryos. Statistical significance analyzed using Mann-Whitney nonparametric test; 40-48 hpf $p=0.043$. **(E)** TEM images showing the apical portion of the neural retina and the sub-retinal space, where tangential processes are observed (yellow arrowheads). At 48 hpf, processes appear electron-dense because of APEX-GBP detection on *crx:GFP*-positive cells. NR: neural retina; RPE: retinal pigmentary epithelium. Scale bars: A, $3 \mu\text{m}$; B, $5 \mu\text{m}$; C, $10 \mu\text{m}$; E, 500 nm .

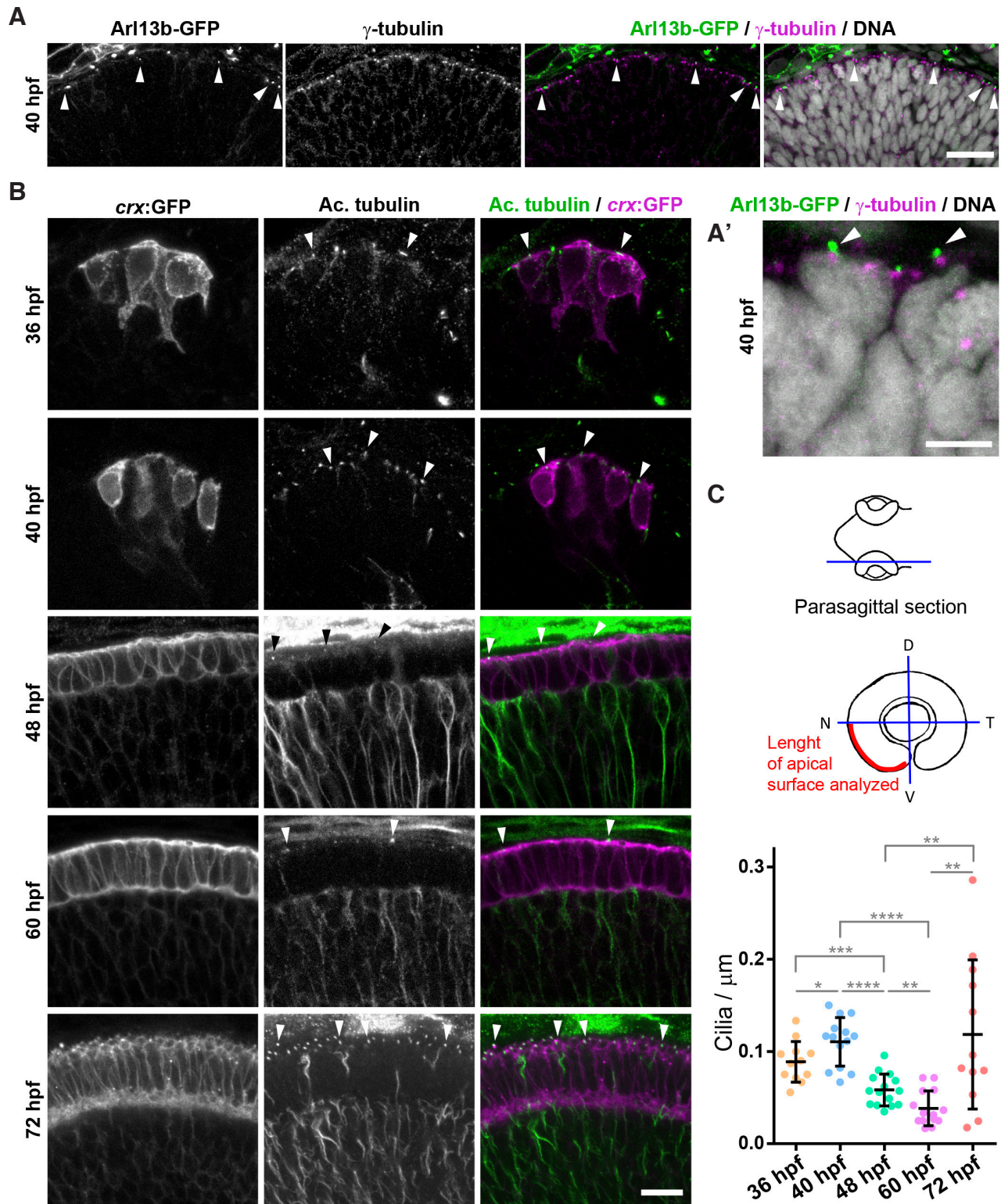


Fig. 4. Presence of primary cilia on photoreceptor progenitors. (A) Confocal image (maximum intensity projection of 2 sections, 1 μ m separation) of the apical region of a 40 hpf zebrafish retina, where cilia are transgenically labeled by Arl13b-GFP (arrowheads) and centrosomes/basal bodies with an antibody to γ -tubulin. In A', a higher magnification from another section is shown, where two short cilia associated with basal bodies are clearly localized at the apical portion of putative photoreceptor progenitors. **(B)** A similar signal is observed by immunolabeling cilia with an anti-acetylated tubulin antibody on crx:GFP transgenic embryos. Very short cilia can be detected at the apical side of photoreceptor progenitors at all stages observed (arrowheads). **(C)** Quantification of the number of cilia along a line spanning the nasal-ventral quarter of the retina on single confocal sections. Mean \pm SD are represented by lines. Statistical significance was determined using the Student's t test. Scale bars: A, 20 μ m; A', 5 μ m; B, 10 μ m.

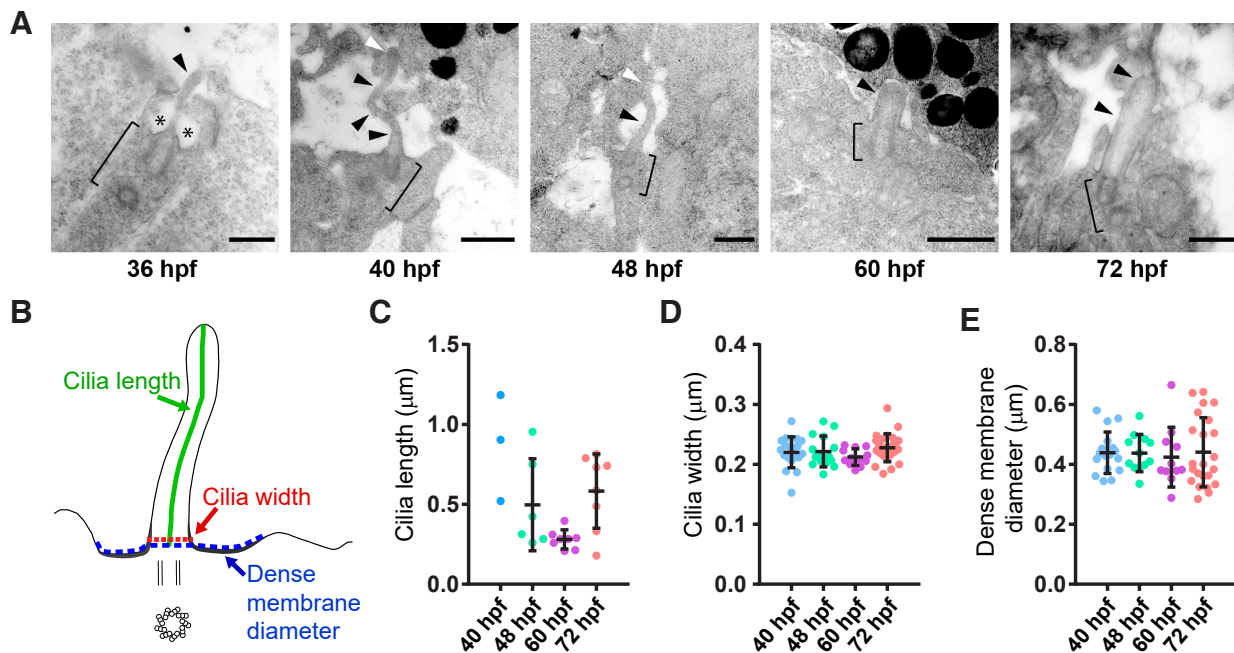


Fig. 5. Ultrastructural characterization of primary cilia on photoreceptor progenitors. (A) TEM images of ultrathin sections from the apical region of zebrafish retinas at different developmental stages, showing typical primary cilia (arrowheads), all of which are on the apical cell membrane and directed towards the sub-retinal space. At 36 hpf, the cell could not be identified, and the cilium shown probably belongs to a neuroepithelial cell. This cilium presents a deep ciliary pocket (asterisks). Between 40 and 60 hpf, most cilia present on putative photoreceptor progenitors are characterized by the absence of a ciliary pocket, and only very few and extremely short cilia could be detected at 60 hpf. At 72 hpf, photoreceptor cilia were usually larger than at earlier stages. Brackets: basal bodies. (C-E) Quantification of primary cilia length, width (at their base) and diameter of the periciliary electron-dense membrane, measured on ultrathin sections imaged by TEM. The drawing in (B) graphically illustrates the measured parameters. Mean \pm SD. Scale bars: 500 nm.

many photoreceptor precursors exhibited a high cell cortex activity, with relatively long, thin processes mostly extending from the apical side, and a few arising from basal-lateral regions (Fig. 2 A-C, Fig. 3A and Supplementary Videos 1, 3, 4 and 5). The highly dynamic nature of these processes can be easily appreciated in Supplementary videos 4 (early-stages *atoh7*:GFP labeling) and 5 (*crx*:GFP). In the anterior-ventral area of 36 hpf retinas, as well as at the periphery of the differentiating cell patch at later stages, isolated *crx*:GFP-positive cells appeared separated from others by a relatively short distance. Some of these cells displayed irregular shapes, with prominent cell protrusions along the apical surface (Fig. 3B and Supplementary Videos 6 and 7). A bit later, at 40 hpf, it was common to see thin, and sometimes branched, processes extending very near and parallel to the apical surface, apparently connecting labeled cells (from here called “tangential processes”; Fig. 3B and Supplementary Video 8). At 48 hpf, a similar behavior was observed in the youngest progenitors, around the periphery of the *crx*:GFP-positive patch of cells (Fig. 3C), but not at 60 hpf. These highly dynamic processes were apparently more numerous at 40 (5-7 simultaneously per cell) than at 36 and 48 hpf (3-4 per cell), but presented similar average lengths of around 3 μ m along these stages (Fig. 3D). Ultrastructural observations showed that these tangential processes were extremely thin (around 0.2 μ m in diameter), and extended from the apical membrane of *crx*:GFP-expressing cells into the sub-retinal space (Fig. 3E). Occasionally, the tangential processes were observed to closely contact other neural retina, as well as RPE cells. Remarkably, at 48 hpf, the sub-retinal space appeared to contain many processes crossing

the retinal apical surface in all directions (Fig. 3E).

We have described here several previously unknown features of the very early photoreceptor differentiation process, which happen in pre-mitotic stages: the early retraction of a basal process, while the cell nucleus is basally positioned; an apical translocation of the cell nucleus; and the formation of highly dynamic cell processes once photoreceptor progenitors are in position at the ONL, largely from the apical side of the cell and extending across the subretinal space (tangential processes).

Presence and role of primary cilia in photoreceptor progenitors

Bearing in mind that the connecting cilium is essential for the extension of the photoreceptor cell outer segment post-mitotically, and that primary cilia are necessary in proliferating retinal progenitors to ensure the correct balance between RGCs and photoreceptor cells (Lepanto, Davison, *et al.*, 2016), we wondered if *crx*:GFP-expressing photoreceptor precursors would have a primary cilium, and if there is a particular cellular localization and a functional role for this organelle during the formation of the ONL. The transgenic labeling by the expression of Arl13b-GFP (Borovina *et al.*, 2010) together with an immunodetection of γ -tubulin at 40 hpf, revealed the presence of several cilia at the outer retinal surface (Fig. 4A). By labeling acetylated tubulin on *crx*:GFP transgenic embryos, we found that, in all observed cases, cilia were present at an apical localization in photoreceptor progenitors at 36 hpf, and that this localization was maintained through different stages up to 72 hpf (Fig. 4B). The density of cilia at the apical border of the neuroepithelium was maintained (or slightly increased) between 36 and

40 hpf, being that at the former most of the cilia corresponded to non-specified neuroepithelial cells and at the latter, to photoreceptor progenitors (Fig. 4C). Beyond 40 hpf, this density decreased steadily until 60 hpf, with a new apparent increase by 72 hpf (Fig. 4C). The ultrastructural analysis demonstrated that at all these stages, cilia observed on photoreceptor precursors were directed towards the sub-retinal space and had the classical conformation of primary cilia (Fig. 5A). Contrary to what we previously described for neuroepithelial cells and RGC progenitors (Lepanto, Davison, *et al.*, 2016), most cilia found on putative photoreceptor progenitors between 40 and 60 hpf sat on a relatively flat area of the apical membrane, with no evident ciliary pocket (Fig. 5A). In addition to becoming scarcer, cilia showed a tendency to turn shorter along this developmental period (Fig. 5A,C). At 72 hpf, when all photoreceptor cells are already post-mitotic and starting to grow their outer segments, cilia length appeared to increase again (Fig. 5A,C). These late cilia were wider in their central-distal portion, indicating the onset of outer segment extension (De Robertis, 1956). They also usually presented a partial or complete ciliary pocket (Fig. 5A,C). In spite of these conspicuous changes in length and general shape, two parameters were maintained constant: the diameter of cilia at their base, and that of the electron-dense area of the periciliary plasma membrane (Fig. 5D,E).

To test for the possible functions of primary cilia in the early stages of photoreceptor cell polarization and differentiation, we treated embryos to severely disrupt cilia using a combination of MOs directed to block the mRNA splicing of two different proteins involved in ciliogenesis: Elipsa and IFT88 (characterized in Lepanto, Davison, *et al.*, 2016). The rationale behind this double-morphant experiment is that even if each of these affected genes might have extra-ciliary functions in the cell (Bizet *et al.*, 2015; Boehlke *et al.*, 2015; Borovina and Ciruna, 2013), they share roles only in cilia formation and maintenance, in addition to the observation that their individual mutants present cilia-specific phenotypes, characterized by a severe ventral curvature of the whole body, and reduced eyes (Omori *et al.*, 2008; Taschner *et al.*, 2016; Tsujikawa and Malicki, 2004). Hence, by using a combination of low doses of splice-blocking MOs, which previously showed not to have conspicuous phenotypes when injected individually, we obtained a strong and specific cilia-disruption phenotype (Lepanto, Davison, *et al.*, 2016; Fig. 6A). As previously described by us, the neural retina of treated embryos was smaller and had fewer cells than in controls, with a remarkable general delay in cell differentiation (Lepanto, Davison, *et al.*, 2016). In that work, we specifically concentrated on RGCs, but here we used *crx*:GFP transgenic expression to follow the dynamic behavior of photoreceptor progenitors upon cilia-impairment. We found that in morpholino-treated embryos, these cells still formed a tight layer of cells that appeared to be correctly polarized and localized at the apical-most aspect of the retina (Fig. 6B and Supplementary Video 9). An increase in image brightness, however, revealed that all along the registered period (36–53 hpf approximately), many of the photoreceptor progenitors presented long and thin basal processes, a feature seldom seen in control cells beyond the earlier stages (Fig. 6B and Supplementary Video 9; compare to data shown in Fig. 2). These processes appeared to be detached from the basal surface, and displayed a dynamic behavior characterized by alternating periods of elongation and retraction, as visualized in time-lapse confocal images (Fig. 6C and Supplementary Video 10). In all observations made, they ap-

peared not to extend beyond the apical border of the RGCs layer (Suppl. Fig. S1). The dynamic changes in these basal processes were such that cells eventually presented two or more processes, sometimes branched, with alternating periods of extension and retraction (Fig. 6C and Supplementary Video 10). In both control and morpholino-treated retinas, photoreceptor progenitors stopped cell process extension during cell division (Supplementary Video 11).

To further analyze the behavior of these aberrant basal processes, we quantitatively compared their occurrence and dynamics in control and morphant embryos. At 36 hpf, basal processes of variable length were extended from *crx*:GFP-positive in both situations, although they were significantly shorter in controls (Fig. 6D). At 53 hpf, however, very few basally-directed cell processes could be detected arising from the ONL in control embryos, and the few that could be measured were much shorter than the several more observed in cilia-impaired retinas (Fig. 6D). At every time point between 36 and 53 hpf, retinas from control and cilia-impaired embryos presented *crx*:GFP-positive basal processes of varying length. In the case of controls, individual basal processes could only be reliably followed for approximately the first four hours (up to 40 hpf), which is graphically represented in Fig. 6E. Here, the average process length at 36 hpf was around 5 μm , while by 40 hpf it was around 3 μm , showing a tendency to becoming shorter as development of the outer nuclear layer proceeded. In treated embryos, on the other hand, we could follow several basal processes until the end of the recorded period (53 hpf). These processes were much longer in average (around 10 μm), and with a greater variation. Both average and standard deviation were maintained along the 17 hours of time-lapse in morpholino-treated embryos (Fig. 6E). In addition, the length of the basal processes in each cell varied prominently along time in both control and morpholino-treated situations, although both the average length and standard deviation was again much higher in the latter (Fig. 6F).

We have here shown the presence of primary cilia localized at the apical border of photoreceptor progenitors. Our initial quantitative analysis of the dynamics and ultrastructure of these cilia suggested possible roles during the early, pre-mitotic stages of photoreceptor cells differentiation. We had previously demonstrated an imbalance in the number of photoreceptor cells at the expense of RGCs when impairing cilia by the simultaneous knockdown of *ift88* and *elipsa* (Lepanto, Davison, *et al.*, 2016). In the present work, we described a novel phenotype on photoreceptor progenitors, characterized by the prolonged presence of dynamic basal processes.

The role of N-cadherin in the organization of the outer nuclear layer and early photoreceptor cell differentiation

With the aim of starting to understand the possible functions of the adhesion molecule N-cadherin in the epithelial-like organization of photoreceptor progenitors in the zebrafish neural retina, we knocked down its expression using extensively characterized morpholino oligomers that have been shown to largely phenocopy the null mutants (Lele *et al.*, 2002) (Fig. 7A). To have a more complete assessment of cell behavior in the neurogenic retina, we performed these knock-downs on double transgenic *crx*:GFP/*atoh7*:gap-RFP (*atoh7*:RFP) embryos (Fig. 7B). This double labeling allowed us to visualize and differentiate the photoreceptor cell layer from the other cell types in the retina, especially other early-born neurons such as retinal ganglion, amacrine and horizontal cells. In addition, bipolar cells, which are late-born neurons also expressing Crx,

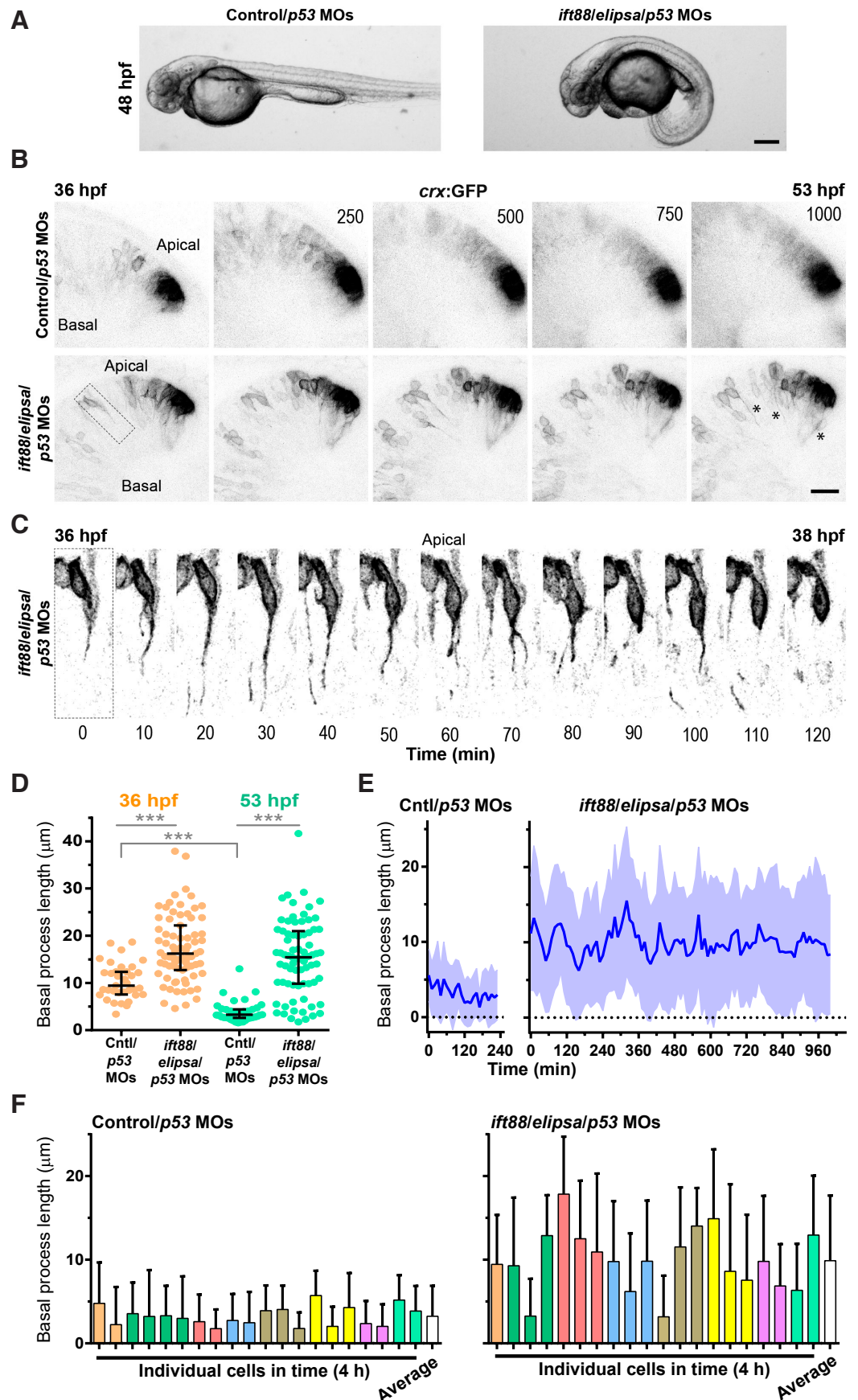


Fig. 6. Effect of primary cilia disruption on photoreceptor progenitors. (A) Cilia disruption using morpholino oligomers (MOs) to *Elipsa* and *IFT88* caused a clear “cilia defect” phenotype on zebrafish embryos. (B) Maximum intensity projection from a time-lapse confocal observation of control and morphant embryos, between 36 and 53 hpf. Long basal processes remain all along the observation time in morphants (asterisks). (C) Higher magnification and thinner projection of the cell squared in B, to show all time points in a two-hour period. The basal process is seen to rapidly change in length and shape during this short period. (D) There is a significant decrease in basal process length (median \pm interquartile values) in control embryos between 36 and 53 hpf, but not in treated embryos (Mann-Whitney test). In both stages, basal processes are significantly longer in morphants. $N=5$ processes/embryo, from 7 control and 15 morphant embryos at 36 hpf; 8 and 15 embryos, respectively, at 53 hpf (3 independent experiments). (E) Averaged (mean \pm SD) length of basal processes measured at each time point from individual cells, for 4 hours in controls and 17 hours in morphants. Between 2 and 4 cells/embryo were manually tracked, measuring the length of the basal process on confocal stacks. $N=20$ cells from 8 embryos; 3 independent experiments in controls, 2 in morphants. (F) Analysis of the averaged basal process length (mean \pm SD) for each cell along the first 4 hours of time-lapse, using the same data as in E. Bars represent individual cells, and each color a different embryo; white bars represent the averaged values. Scale bars: A, 200 μm ; B, 20 μm ; C, 8 μm .

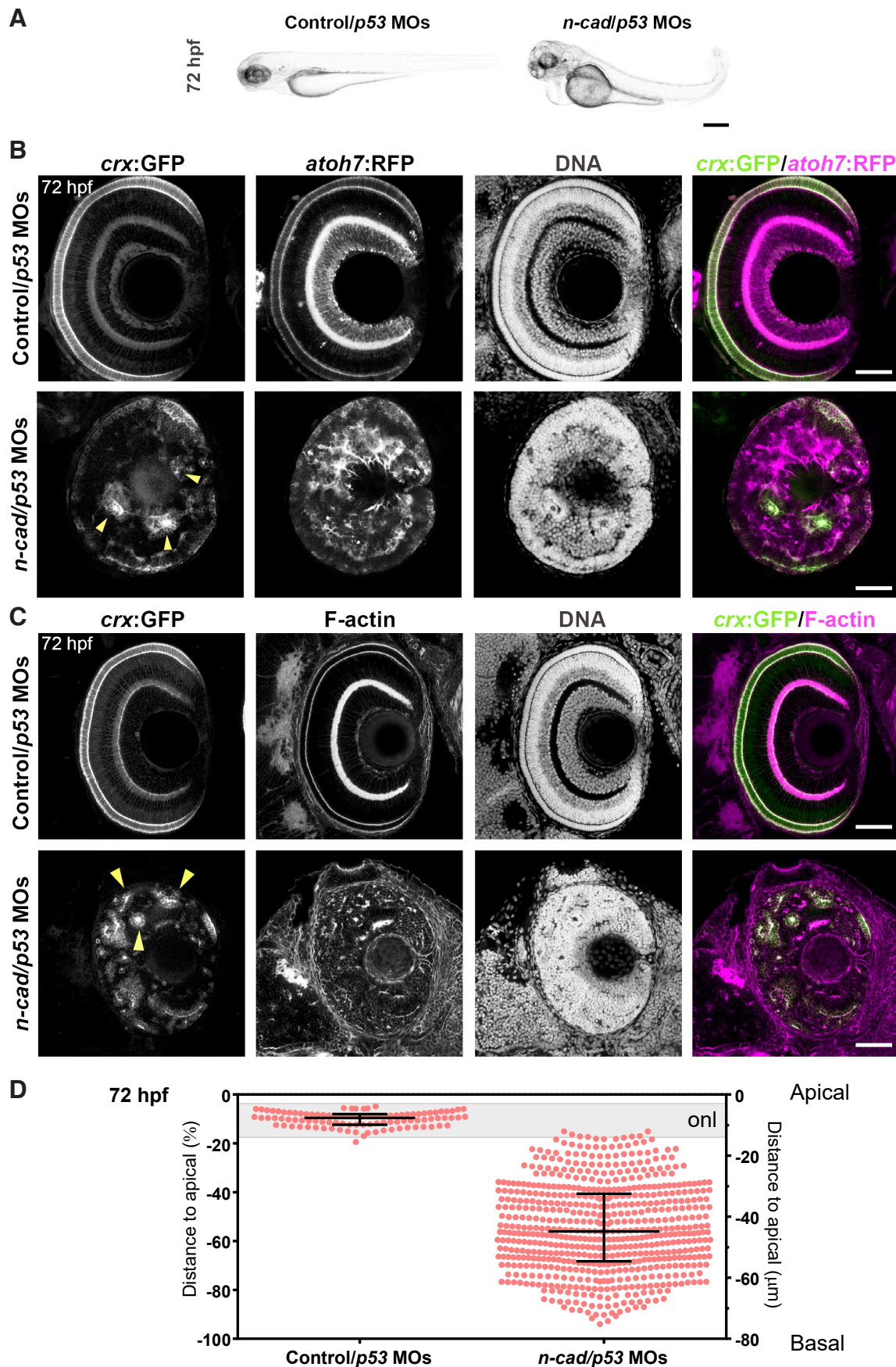


Fig. 7. Effect of N-cadherin knock-down on the formation of the outer nuclear layer. (A) External phenotype of an N-cadherin morphant (*N-Cad*) at 72 hpf, compared with a control embryo. **(B)** Single confocal sections of the retina from 72 hpf *crx*:GFP/*atoh7*:RFP double transgenic zebrafish embryos injected with the *N-Cad* or control MOs, labeled with methyl green (DNA). A severe disruption in retinal layering is observed in morphant embryos, characterized by the formation of multiple photoreceptor-only rosettes (arrowheads). **(C)** Single confocal sections of the retina from 72 hpf *crx*:GFP transgenic embryos injected with the *N-Cad* or control MOs, labeled with TRITC-phalloidin (F-actin) and methyl green (DNA). **(D)** Representation of the position of photoreceptor cells along the apico-basal axis of the retina, in control and *N-Cad* morphants at 72 hpf. The distance of the cell nucleus from the apical surface (position "0") was normalized as a percent of total retinal width. Median \pm interquartile values are shown. $N=100$ control and 629 morphant cells; from 20 control and 30 morphant embryos; 5 independent experiments. The scale on the right shows the average width of the retina in controls (80 μ m), which was indistinguishable from that of morphants (median of 80.4 and 81.2 μ m, with SD of 11.5 and 10.5 μ m, respectively). The gray band represents the approximate position of the ONL ("onl") in control embryos. Scale bars: A, 300 μ m; B and C, 50 μ m.

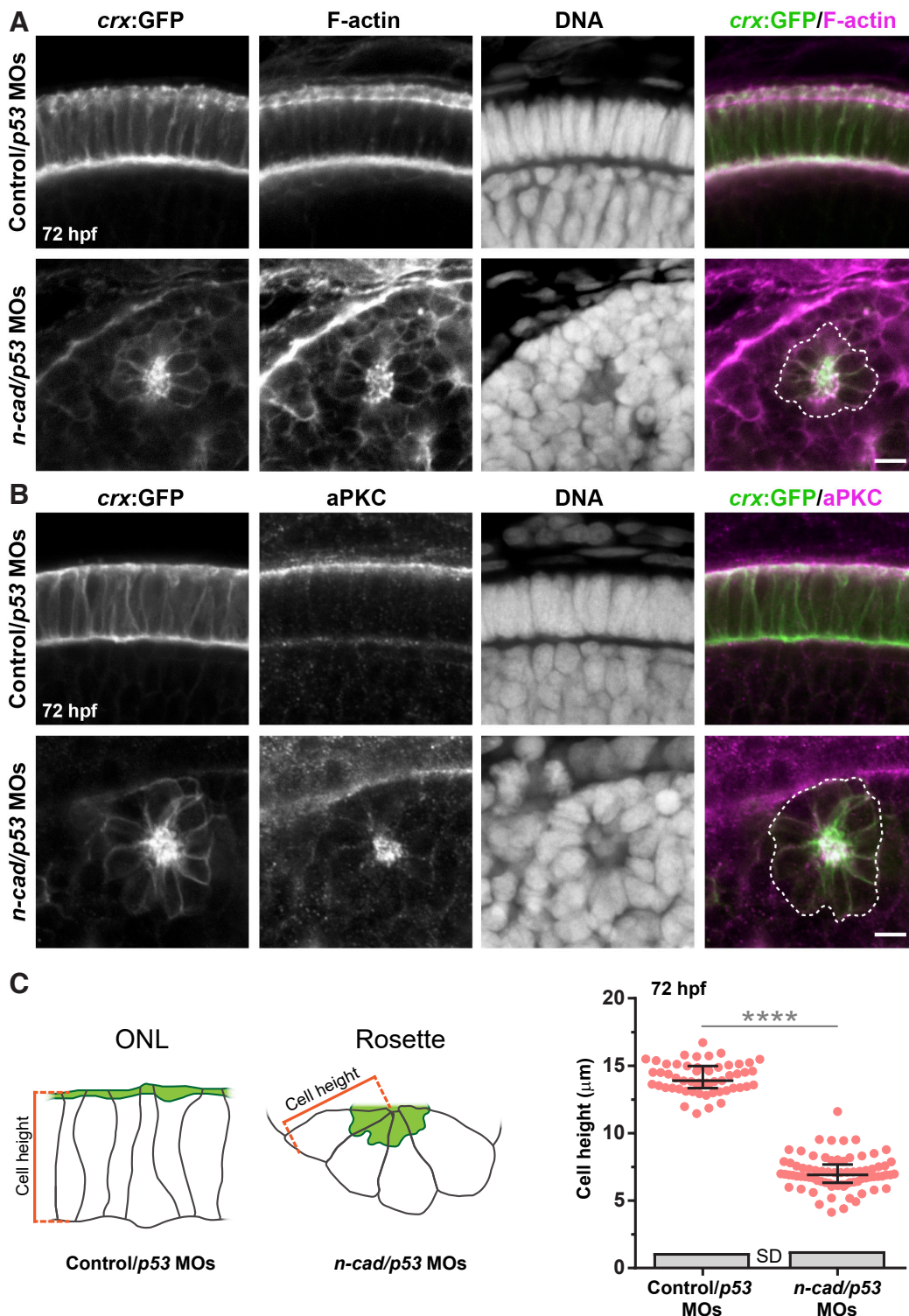


Fig. 8. Effect of N-cadherin knock-down on photoreceptor cell morphogenesis.(A,B) High magnification confocal sections of the retina from control and N-Cad MO-injected *crx:GFP* transgenic embryos at 72 hpf, labeled with TRITC-phalloidin (F-actin; A), anti-aPKC ζ antibody (aPKC; B) and methyl green (DNA). Rosette-like groups of photoreceptor cells (demarcated with the white dashed line) are observed, where both F-actin and aPKC accumulate at the center. (C) Comparative quantification of the height (apico-basal length) of photoreceptor cells in control and N-Cad morphant embryos at 72 hpf. N=55 control and 77 morphant cells; 10 control and 14 morphant embryos; 4 independent experiments. Median and interquartile range are shown; gray bars represent the standard deviation (SD); statistical significance was determined using the Mann-Whitney test. Scale bars: 5 μ m.

are not labeled by *atoh7:RFP* and can thus be differentiated from photoreceptor progenitors. At 72 hpf, we observed the expected general disruption of retinal tissue organization, with the appearance of both ectopic *atoh7:RFP* and *crx:GFP* signal (Fig. 7B). Interestingly, the strongest signal in each case (RGCs and photoreceptor cells, respectively), appeared to be completely segregated. Similar observations could be obtained after labeling *crx:GFP* embryos for F-actin, which is normally accumulated at plexiform layers at this stage (Fig. 7C). In morphant embryos, most photoreceptor cells were grouped in small round structures, with a rosette-like appearance. To have a quantitative idea of photoreceptor cell misplacement, we measured the distance from the cell nucleus to the apical surface in 72 hpf retinas (Fig. 7D). While in control embryos photoreceptor cells were confined to the outer nuclear layer, within 14–15 μ m from the apical surface, in N-cadherin morpholino-treated embryos we found an enormous dispersion of the cells across the apico-basal axis. In this case, however, photoreceptor cell distribution presented a preference for the central one-third of the retina: 50% of the *crx:GFP*-positive photoreceptor cells were localized between 40.6 and 68.3% of the retinal width in morphants, against 8–12.4% in controls (Fig. 7D).

At higher magnification, the rosette organization of photoreceptor cells in N-cadherin morphants was more evident (Fig. 8A,B). In these structures, photoreceptor cells appeared wedge-shaped, with a smaller portion towards the center of the rosette, and a wider side towards the periphery. Both F-actin and the polarity marker aPKC ζ were accumulated at the central portion, indicating an apical identity of this region (Fig. 8A,B). As expected, this notorious shape

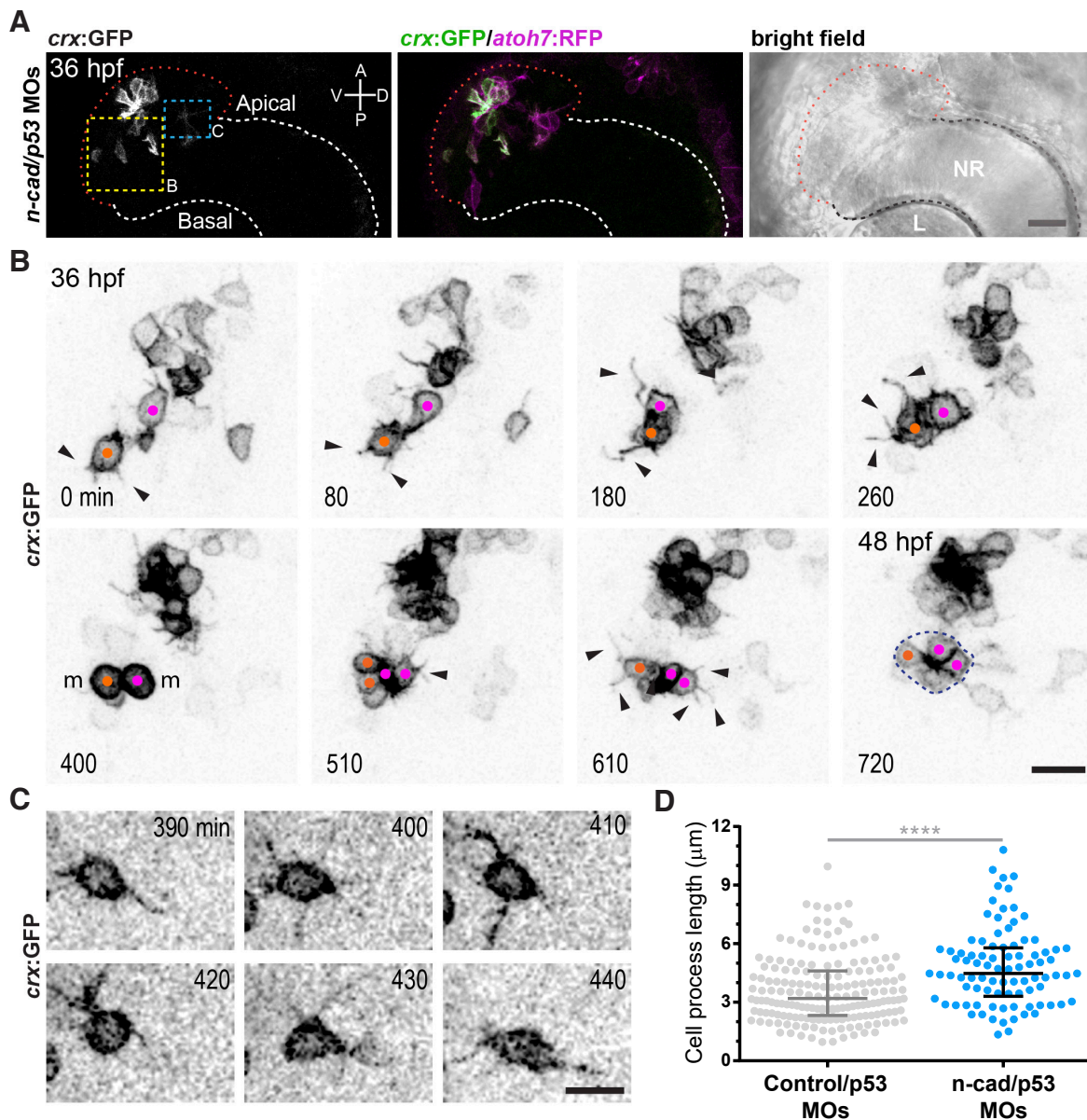


Fig. 9. Effect of N-cadherin knock-down on the dynamics of photoreceptor progenitors. **(A)** Low magnification confocal images of the beginning of the time-lapse analyzed in B and C, at the level of the anterior region of an N-cadherin morphant retina, from a *crx:GFP/atoh7:RFP* double transgenic embryo. L: lens; NR: neural retina. White dashed line: limit of the neural retina; red dashed line: apical limit of the aberrant anterior-ventral area of the retina. **(B)** Detail of confocal time-lapse experiment showing the process of rosette formation by ectopic photoreceptor progenitors (yellow dashed area in A). The color dots indicate individual cells that join to form the rosette, and their respective daughter cells. These cells mitotically divide at the same time (m). Arrowheads: cell processes. **(C)** Magnified image of another region of the same time-lapse (blue dashed area in A), showing a single *crx:GFP/atoh7:RFP*-positive cell at different time points, to better visualize the neurite-like processes. **(D)** Quantification of photoreceptor progenitors cell process length in N-cadherin morphants at 40 hpf, compared with the length of tangential processes in normal embryos (control data are the same as in Fig. 3D). N-cadherin morphants $N=89$ processes; 8 embryos; 3 independent experiments. Median and interquartile range are indicated; statistical significance determined using the Mann-Whitney test. Scale bars: A, 20 μm ; B and C, 10 μm .

change made photoreceptor progenitors in rosettes significantly shorter along the apico-basal axis than their control counterparts, localized at the ONL (Fig. 8C). However, when analyzing the dispersion of cell height between cells in each situation, they were surprisingly constant, indicating that the general photoreceptor cell morphogenesis was not affected by N-cadherin knock-down. To further analyze the process that leads to this ectopic position and aberrant organization of the photoreceptor progenitors in N-

cadherin-impaired retinas, we followed the behavior of these cells since 36 hpf on *crx:GFP/atoh7:RFP* double transgenic embryos by time-lapse confocal microscopy (Fig. 9). At these earlier stages, differentiation is only evident at the anterior-ventral portion of the retina, and this is where structural disruption was also evident in N-cadherin morphants, as a wide extension of the retinal tissue beyond the apical border (Fig. 9A and Supplementary Fig. S2). Photoreceptor progenitors could be unambiguously detected from very

early stages because they were doubly labeled by GFP and RFP. In morphants, they were usually first detected in central regions of the retina and then started to display random short movements, eventually leading to some displacement, showing a high degree of cell cortex activity as seen in control embryos (Fig. 9B,C; Supplementary Fig. S2, and Videos 12-15). We thus wondered how photoreceptor cell rosettes are formed in the N-cadherin morphants. Fig. 9B, and Supplementary Video 12, show how two initially isolated *crx*:GFP-positive cells approach and attach, being joined by other cells to form an identifiable rosette in approximately 12 hours. Interestingly, both cells divided at the same time, around 5-6 hours after binding, which is comparable to the quantified time of the first cell division of *crx*:GFP-positive progenitors after arriving to the ONL in control embryos (see Fig. 2G). Supplementary Fig. S2A and Video 14 illustrate another example of the process of rosette formation. As photoreceptor progenitors displaced in the retina, they usually extended profuse neurite-like cell processes, similar to the tangential processes we observed in control embryos (Fig. 9C and Supplementary Fig. S2B; Supplementary Videos 13 and 15). A quantification of the length of these processes found in many ectopic *crx*:GFP-positive cells, either isolated or in rosettes, indicated that they are slightly but significantly longer than the tangential processes measured in controls at 40 hpf (Fig. 9D).

Finally, in order to better characterize the behavior of photoreceptor progenitors in N-cadherin knock-down retinas, we tracked the trajectories of these cells from the moment they were first detected by *crx*:GFP expression to the inclusion in a rosette, as this is the event that marks the attachment to other photoreceptor progenitors (and hence, ontogenetically analogous to the inclusion in the ONL). Even if they did not translocate for long distances, the observed cells displayed apparently random movements, with

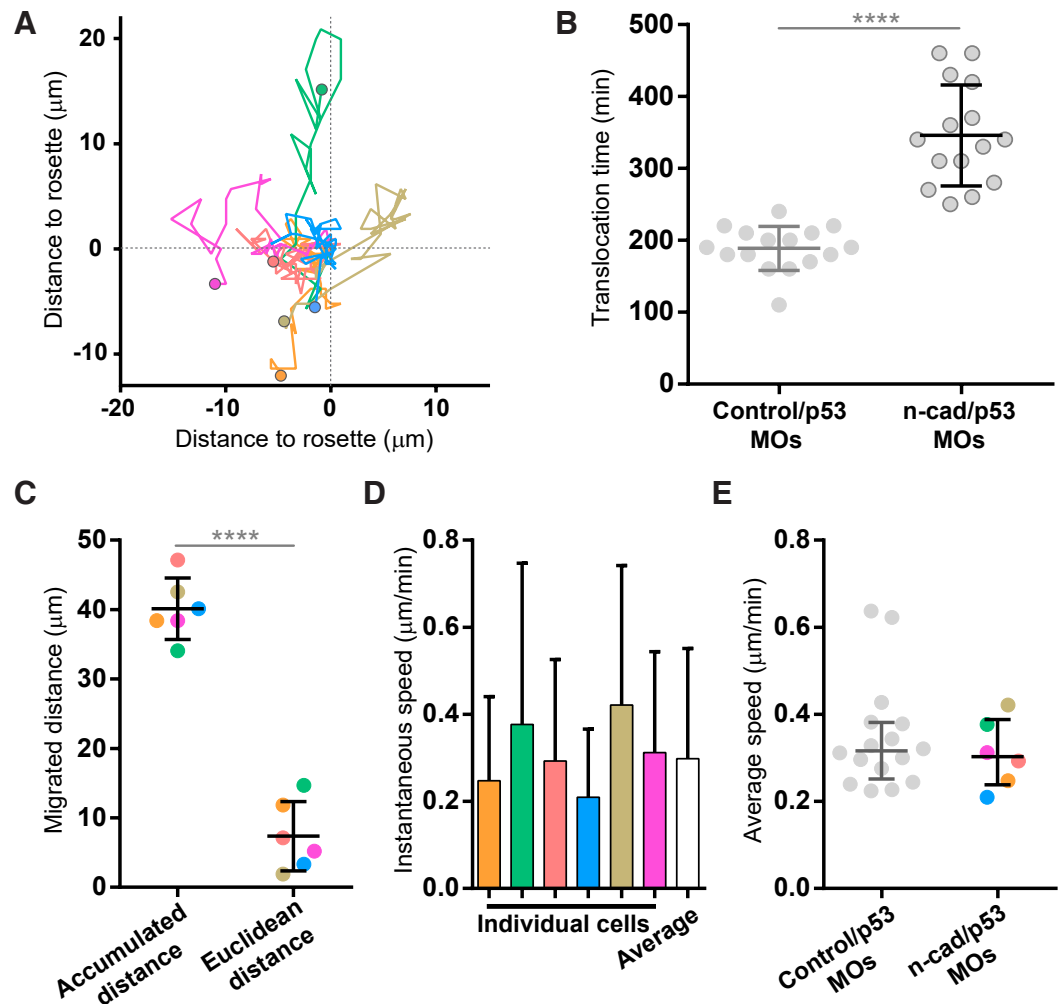


Fig. 10. Quantitative analysis of ectopic photoreceptor progenitor dynamics in N-cadherin morphants. (A) Tracked trajectories (x-y) of 6 *crx*:GFP-positive cells (3 embryos, 2 independent time-lapse experiments), from the onset of GFP detection to their positioning at a rosette. All trajectories are aligned to the final position (0 μm in both axes) and the starting point is marked with a colored dot. **(B)** Comparison of the time that *crx*:GFP-positive cells take to become inserted in the ONL (Control) or in a rosette (N-Cad MO), since the time GFP signal becomes detectable. Control data are from the same data set analyzed in Fig. 2E-F, and N-Cad MO data are the same as A in this figure. Mean ± SD; statistical significance determined using the Student's t test. **(C)** Comparison of the total distance migrated by photoreceptor progenitors (Accumulated distance) with the effective displacement (Euclidean distance) in N-cadherin morpholino-treated embryos. The data used for this calculation were the same as in A, maintaining the color code for cell identification. Mean ± SD; statistical significance determined using the Student's t test. **(D)** Instantaneous speeds of photoreceptor progenitors from A (same color code), averaged along the whole time. White bar: averaged instantaneous speeds of all cells. Mean ± SD. **(E)** Comparison of the average speed of migration in N-cadherin morphants (N-Cad MO) to the translocation speed in normal (Control) embryos, as shown in Fig. 2F. Median ± interquartile range; medians not statistically different according to Mann-Whitney test.

different speeds and directions (Fig. 10A). We also compared the time it took the morphant photoreceptor cells to reach a rosette, to that of controls to translocate to the ONL, finding it was significantly longer (nearly double: 346 ± 70 against 189 ± 31 min, respectively) (Fig. 10B, and see also Fig. 2 for more data on untreated embryos). The effective displacement (Euclidean distance between the starting and destination points) was in all cases much shorter than the total distance migrated (Fig. 10C), which is strong indicator of a random movement. Also using the data from the tracked trajectories, we could determine the instantaneous and average speeds

of these cells while migrating (Fig. 10 D,E). Similarly to what we describe above for apical translocation in normal retinas, there was a high level of variability in cell speed at different time points (Fig. 10D, compare to Fig. 2F), and somehow surprisingly, the average migration linear speed in N-cadherin-treated embryos was statistically undistinguishable from the translocation linear speed in normal embryos, with median values around 0.3 $\mu\text{m}/\text{min}$ (Fig. 10E).

By using live confocal microscopy analysis of *crx*:GFP/*atoh7*:RFP double transgenic zebrafish embryos, we were able to describe with an unprecedented spatial and time resolution the early stages of photoreceptor cell differentiation in N-cadherin-impaired embryos. We surprisingly found that, despite the great distortion of retinal architecture observed in these embryos, photoreceptor progenitors exhibited a morphological differentiation and cellular dynamics comparable to those of control embryos, rapidly migrating while displaying cell processes, until they polarized at the ectopic rosettes.

Discussion

Previous research on vertebrate photoreceptor cell differentiation has largely concentrated either on the initial cell fate decisions that give place to the generation of committed progenitors (see for example Boije *et al.*, 2014), or on the maturation and differentiation of the outer segment (Whewey *et al.*, 2014). In the present work, we decided to start filling the gap between these two processes that are not only apart in terms of cell differentiation stages, but also in time, since one of the most salient particularities of differentiating photoreceptor cells is the long time they spend between specification (highlighted by the expression of distinctive markers such as *Crx*; Shen and Raymond, 2004) and actual cell differentiation (Crespo and Knust, 2018). Remarkably, cones are among the first cell types to be specified in the retina, even sharing the expression of the proneural transcription factor *Atoh7* with the first neurons to become post-mitotic, RGCs (Boije *et al.*, 2014). RGCs start to differentiate a very short time after the last cell division at the apical side of the neuroepithelium. The stereotyped differentiation process of these cells occurs in a few hours in the zebrafish, and it does not include an “unpolarized” stage, but a gradual transition in which the nascent neuronal polarity overlaps with the fading epithelial polarity (Zolessi *et al.*, 2006). We have demonstrated here some relevant differences in the way photoreceptor cells differentiate: first, cycling photoreceptor progenitors translocate their nuclei and accommodate at the final place of differentiation many hours before becoming postmitotic (our quantification shows $6:25 \pm 1:06$ h to the first cell division, which happens around 48 hpf, and Weber *et al.*, 2014, showed that the second and last cell division occurs 12-24 hours after this); second, cell body translocation to reach this position is apical-ward, and they detach from the basal lamina to retract a basal process; third, once at the apical side, and albeit showing evident signs of polarization such as an apical cilium and adhesion complex molecules, they spend several hours extending multiple neurite-like cellular processes along the sub-retinal space. These tangential processes, which to our knowledge have not been previously described, are rather remarkable in cells that when mature only have a very short axon and no dendrites, and are reminiscent of the unpolarized stage 2 of rat hippocampal neurons in culture (Cáceres *et al.*, 2012). We

have previously shown that RGCs can also display this type of behavior in culture, or *in vivo* when lacking a positional signal for axonogenesis, such as Laminin1 (Randlett *et al.*, 2011). Interestingly, the tangential processes in photoreceptor progenitors appear to peak in number and length around the time when the ONL is being assembled, to stop by around the time photoreceptor cells undergo their last cell division and start to elongate their bodies after 60 hpf. It is tempting to speculate that they might have a function in establishing contacts between early photoreceptor cells, helping in migration and leading to their organization in the crowded and highly regular ONL. In support of this supposition, we showed here that isolated ectopic photoreceptor progenitors in N-cadherin morphants display longer neurite-like processes before and during the establishment of rosettes. A relatively similar behavior was recently described for differentiating spinal cord neurons, which extended dynamic processes tangential to the basal surface of the neuroepithelium, just before axon outgrowth (Hadjivasiliou *et al.*, 2019). Interestingly, these processes were shown to mediate lateral inhibition through Delta-Notch signaling. Although they were only two, directed in opposite directions, and much longer (one order of magnitude in average) than the photoreceptor cell tangential processes described here, it is tempting to speculate on analogous functions.

Motivated by the observation by us and others (see for example Crespo and Knust, 2018) of an early, pre-neurogenic, epithelial-like polarity of photoreceptor precursor cells, we decided to explore the possible roles of two conspicuously polarized structures in the retinal neuroepithelium: the primary cilium and the sub-apical N-cadherin-based adhesion complex. Primary cilia have been shown to have different functions in neuronal differentiation, including modulating aspects such as cell proliferation, cell determination, cell shape and neuronal migration (Higginbotham *et al.*, 2012; Lepanto, Badano, *et al.*, 2016). We describe here the presence of relatively short primary cilia, located at the apical membrane of photoreceptor progenitors, which can be differentiated from those of neuroepithelial cells by their apparent lack of a complete ciliary pocket (Lepanto, Davison, *et al.*, 2016). These cilia get shorter and scarcer as development proceeds, to nearly disappear by 60 hpf, clearly indicating that they are not the direct precursors of the outer segment, a structure that starts to form by around 72 hpf (Branchek and Bremiller, 1984). Early primary cilia did not appear to be essential for the orientation of photoreceptor progenitors or the formation of an ONL, as seen upon their disruption using a previously characterized combination of morpholinos to ciliogenesis-involved proteins. These morpholinos, acting together, cause the knock-down of two independent intraflagellar transport proteins, IFT88 and Elipsa giving a very reliable and reproducible phenotype, with no evident off-target effects (Lepanto, Davison, *et al.*, 2016). Similar to what was described in that previous work, this treatment generated a severe growth and cell differentiation delay in the retina, where all cell types are reduced in number, but maintaining the laminar organization. By using the *crx*:GFP reporter, we could describe here a very remarkable novel effect of cilia disruption on the process of basal processes retraction in photoreceptor progenitors. Instead of a very quick retraction after detachment observed in the untreated condition, in morphants these basal processes remained elongated for several hours, even when photoreceptor cell bodies were normally positioned and divided at the apical retina. An analog phenotype was ob-

served in *Slit1b* morphants on post-mitotic RGCs, which would take longer than usual to detach and retract the apical process, even if differentiating normally at the basal side (Zolessi *et al.*, 2006). One important difference is that the elongated basal processes of photoreceptor cells were in general detached from the basal surface and extremely dynamic in length. Hence, contrary to what was described for RGCs, where the failure to retract was due to a deficiency in N-cadherin down-regulation mediated by the *Slit* receptor *Robo3* (Wong *et al.*, 2012), the maintenance of photoreceptor cell basal processes does not seem to depend on a defect in detachment. Rather, cilia disruption seems to be affecting the shortening of the basal process. At this stage, we cannot ascertain if the observed phenotype is caused cell autonomously, by the disruption of cilia in the affected photoreceptor progenitors themselves, or if it is related to a missing signal from the basal retina, where RGCs are generated in lower than normal numbers (Lepanto, Davison, *et al.*, 2016). This latter idea is supported by the observation that, in spite of their dynamic behavior, basal processes never appeared to extend beyond the apical limit of the ganglion cells layer.

The proper differentiation of most central nervous system neurons requires a down-regulation of epithelial polarity, as was shown for RGCs (Zolessi *et al.*, 2006). In neurons, typical epithelial polarity molecules, such as N-cadherin or *Pard3* are no longer associated to an apical identity and appear to gain new functions in axon specification and neurite outgrowth (see reviews in Gärtner *et al.*, 2015; Hapak *et al.*, 2018). Photoreceptor cells in general (either from vertebrates or invertebrates) have the particularity of presenting, simultaneously, polarity features found in neurons and epithelial cells, providing a very interesting opportunity to understand the roles of apical adhesion complexes in neuronal development and evolution. Here, we concentrated in further characterizing the roles of the adhesion protein N-cadherin on the organization of photoreceptor cells in an ordered layer, and in their polarization or orientation. Like it was previously described for mutants, the downregulation of N-cadherin expression caused a general disorganization of the zebrafish retina, with the extensive formation of cell rosettes, where photoreceptor progenitors polarized with their apical region towards the center (Erdmann *et al.*, 2003; Masai *et al.*, 2003; Wei *et al.*, 2006). Our time-lapse analyses demonstrated that at early stages, and similar to what happens in control embryos, photoreceptor progenitors in morphants for N-cadherin arise from *crx*:GFP/*atoh7*:RFP-expressing cell precursors that individually translocate (in this case, migrate) to eventually join other photoreceptor cells (in this case, in rosettes instead of the ONL). This translocation took, however, the double of time in morphant than in control embryos, suggesting either a direct role for N-cadherin in this process, or that the integrity of neuroepithelial polarity is an important factor. It was also interesting that even if the general architecture of the retina was completely altered by N-cadherin knock-down, these non-polarized and apparently disoriented isolated progenitors were able to recapitulate the initial stages of ONL formation, albeit in a small round structure (a rosette): they joined together, divided a few hours later and much later differentiated acquiring an apparently normal photoreceptor-like cell polarity (at least in initial stages). It must be taken into account that, as described in previous work (Malicki *et al.*, 2003), the effect of N-cadherin mutation or knock-down is largely non-cell autonomous, probably due to

the fact that the functions of cell adhesion imply the binding of a group of cells (an opposite autonomous community effect is also described for larger groups of cells). Hence, our results are limited to the effect of N-cadherin disruption in the whole tissue, and we cannot ascertain at this moment how much of this effect is intrinsic to photoreceptor progenitors, or a consequence of the general cell adhesion failure in the retina. N-cadherin appears then to be necessary in the retina for photoreceptor cells to remain attached to the outer limiting membrane through adherens junctions, but not for these cells to recognize each other and eventually join and correctly polarize. Other adhesion molecules, not analyzed in the present work, could certainly be involved in other aspects of retina and photoreceptor cell morphogenesis (see for example Zou *et al.*, 2012).

Altogether, the findings described in this work reinforce the idea of a complex set of signaling processes involved in sculpting the final functional morphology of neurons, and that each neuron requires a unique set, exquisitely tailored to its particular shape, position and function. The very special case studied here, the vertebrate photoreceptor, may not represent “canonical” neurons, but exactly because of its characteristic of maintaining a combination of epithelial and neuronal polarity features, it becomes a unique opportunity to begin to understand how neurons arise from epithelia, both in development and in evolution.

Materials and Methods

Fish care and breeding

Zebrafish were maintained and bred using standard methods (Lepanto, Davison, *et al.*, 2016). Embryos were raised at 25 to 31 °C depending on the experiments, and staged in hours post-fertilization (hpf). We used wild-type (Tab5) and previously established transgenic lines: Tg(*actb2*:Arl13b-EGFP)hsc5 (Arl13b-GFP), kindly provided by B. Ciruna (Borovina *et al.*, 2010); Tg(*atoh7*:gap43-mRFP)cu2 (Zolessi *et al.*, 2006). All manipulations were carried out following the approved local regulations (CEUA-IPMon, and CNEA).

Injection of molecular constructs and morpholino oligomers (MOs)

We constructed the following vectors using the Multisite Gateway-based (ThermoFisher Scientific) to2 kit system (Kwan *et al.*, 2007) pDestTol2pA2;*crx*:EGFP-CAAX, pDestTol2pA2;*crx*:mCherry-CAAX. p5E-*crx* was kindly provided by R. Wong (Suzuki *et al.*, 2013). The construct *bact2*:APEX2-GBP cloned in a pDESTTol2pA2 was obtained from Addgene (Plasmid 67668) (Ariotti *et al.*, 2015). Plasmid DNA together with Tol2 transposase mRNA (0.5 nL; 2.5 and 6 pg, respectively) were injected at the one-cell stage according to standard techniques. For transgenic line generation, identified carriers were outcrossed until offspring inherited the transgene at mendelian ratios. We generated the following transgenic lines in this work: Tg(*crx*:EGFP-CAAX, *cmlc2*:GFP); Tg(*crx*:mApple-CAAX, *cmlc2*:GFP); Tg(*bact2*:APEX2-GBP, *acrlys*:mCherry).

Previously well-characterized MOs were obtained from Gene Tools (Philomath, USA): *ift88*-SP (AACAGCAGATGCAAAATGACTCACT), which targets the exon 3 - intron 3 boundary of *ift88* (Lepanto, Davison, *et al.*, 2016); *elipsa*-SP (CTGTTTTAATAACTCACCTCGCTGA) which targets the exon 1 - intron 1 boundary of *elipsa* (Lepanto, Davison, *et al.*, 2016); *cdh2*-TR (TCTGTATAAAGAAACCGATAGAGTT) which targets the 5' UTR of the N-cadherin mRNA (Lele *et al.*, 2002). All MOs were injected in the yolk of 1–4 cell-stage embryos, at a maximum volume of 3 nL, 6 ng/embryo of each *ift88* and *elipsa*, and 0.8 ng/embryo of *cdh2*. In the case of *ift88* and *elipsa*, we used a combination of both MOs at doses that we previously showed not to be individually effective in generating either a general or a retina phenotype, in order to avoid eventual extra-ciliary effects

and to only obtain a strong cilia-specific phenotype (Lepanto, Davison, et al., 2016). As a control, we used matching doses of a standard MO (CCTCTTACCTCAGTTACAATTATA) from Gene Tools (Philomath, USA). In all cases, we co-injected the standard anti-*p53* MO (3.2 and 1.6 ng for *ift88/elipsa* and *cdh2*, respectively; Robu et al., 2007).

Immunofluorescence

Embryos grown in 0.003 % phenylthiourea (PTU; Sigma) were fixed overnight at 4 °C in 4 % paraformaldehyde in PBS and subjected to permeabilization and whole-mount immunostaining as previously described (Lepanto, Davison, et al., 2016). Primary antibodies used: anti-acetylated tubulin (Sigma-Aldrich, T-7451), 1/1000; anti- γ -tubulin (Sigma-Aldrich, T6557), 1/500; anti-GFP (DSHB, DSHB-GFP-12A6), 1/200; anti-pan-cadherin (Sigma-Aldrich, C3678), 1/500; anti-aPKC ζ (SCBT, sc-216), 1/500. Secondary antibodies from ThermoFisher Scientific: anti-mouse IgG-Alexa 488 (A11034), 1/1000; anti-mouse IgG-Alexa 555 (A21424), 1/1000; anti-rabbit IgG-Alexa 633 (A21070). All antibody incubations were performed overnight at 4 °C. Nuclei were fluorescently labeled using methyl green (Prieto et al., 2014) and actin filaments with TRITC-conjugated phalloidin (Sigma-Aldrich, P1951). Observation of whole embryos was performed using a Zeiss LSM 880 or a Zeiss LSM 800 laser confocal microscope, with 20x 0.7 NA, 25x 0.8 NA, 40x 1.2 NA or 63x 1.3 NA glycerol:water (75:25) objectives.

In vivo confocal microscopy

Embryos were selected at 36 hpf, anesthetized using 0.04 mg/mL MS222 (Sigma) and mounted in 1 % low melting-point agarose, containing 0.003 % N-phenylthiourea and 0.04 mg/ml MS222/tricaine (Sigma) over n° 0 glass bottom dishes (MaTek). During overnight image acquisitions, embryos were kept in Ringer's solution (116 mM NaCl, 2.9 mM KCl, 1.8 mM CaCl₂, 5 mM HEPES pH 7.2) with 0.04 mg/mL MS222. Live acquisitions were made using a Zeiss LSM 880 laser confocal microscope with a 25X 0.8 NA or 40x 1.2 NA objective and glycerol:water (75:25) immersion medium. Stacks around 50 μ m-thick were acquired in bidirectional mode, at 1 μ m spacing and 512 × 512 pixel resolution every 10 or 15 min. The acquisition time per embryo was approximately 45 s, and up to 8 embryos were imaged in each experiment.

Transmission electron microscopy

Embryos were fixed for 30 min at room temperature by immersion in 4 % paraformaldehyde, 2.5 % glutaraldehyde, 0.1 M phosphate buffer, pH 7.2–7.4. Heads were then dissected and incubated in fixative solution overnight at 4 °C. After washing, they were post-fixed in 1 % osmium tetroxide. APEX2-GBP embryos were processed according to Ariotti et al., 2015. Briefly, embryos were fixed for 30 min at room temperature by immersion in 4 % paraformaldehyde, 2.5 % glutaraldehyde, 0.1 M sodium cacodylate buffer, pH 7.4. Dissected heads were then fixed overnight at 4 °C. After repeatedly washing in buffer, embryo heads were incubated with diaminobenzidine (DAB) in the presence of H₂O₂ for 30 min at room temperature, washed in 0.1 M sodium cacodylate buffer, post-fixed in 1 % osmium tetroxide for 15 min and washed again. In all cases, embryo heads were dehydrated using ethanol, infiltrated and embedded in Araldite resin. Ultrathin 70 nm sections were obtained using an RMC MT-X ultramicrotome, mounted on formvar-coated copper grids and stained with 2 % aqueous uranyl acetate followed by Reynold's lead citrate. Observation and acquisition was performed using a Jeol JEM 1010 transmission electron microscope operated at 80 kV, equipped with a Hamamatsu C4742-95 digital camera or a Jeol JEM 2100 operated at 120 kV, with a GatanOrion 1000 digital camera.

Data analysis

Images were processed and analyzed using Fiji (<https://fiji.sc/>). Statistical analyses were performed using GraphPad Prism 6. As a routine, the datasets were checked for normality using the D'Agostino-Pearson, or the Shapiro-Wilk normality tests. To analyze statistical significance of

differences in average, we performed a Student's *t* test in the case of normal data distribution, and a Mann-Whitney test in the case of non-normal data.

Acknowledgements

We thank Kristen Kwan, Rachel O.L. Wong, Brian Ciruna and William A. Harris for sharing plasmids and/or fish lines; Gabriela Casanova (Unidad de Microscopía Electrónica, Facultad de Ciencias, Udelar), Álvaro Olivera (CURE Rocha, Udelar) and Marcela Díaz/Tabaré De Los Campos (Unidad de Microscopía, Institut Pasteur Montevideo) for technical assistance with microscopy; Gisell González, for her invaluable and continuous support with fish care. This work was partly funded by an ANII-FCE grant to FRZ (1_1_2014_1_4982); SNB PhD fellowship to GA; CAP-Udelar Master's fellowship to MR; FOCEM-Institut Pasteur de Montevideo Grant (COF 03/11); Programa de Desarrollo de las Ciencias Básicas (PEDECIBA, Uruguay).

References

- AMINI R, ROCHA-MARTINS M, NORDEN C (2018). Neuronal Migration and Lamination in the Vertebrate Retina. *Front Neurosci* 11: 742.
- ARIOTTI N, HALL TE, RAE J, FERGUSON C, MCMAHON KA, MARTEL N, WEBB RE, WEBB RI, TEASDALE RD, PARTON RG (2015). Modular Detection of GFP-Labeled Proteins for Rapid Screening by Electron Microscopy in Cells and Organisms. *Dev Cell* 35: 513–525.
- BIZET AA, BECKER-HECK A, RYAN R, WEBER K, FILHOL E, KRUG P, HALBRITTER J, DELOUS M, LASBENNES M-C, LINGHU B, et al., (2015). Mutations in TRAF3IP1/IFT54 reveal a new role for IFT proteins in microtubule stabilization. *Nat Commun* 6: 8666.
- BOEHLKE C, JANUSCH H, HAMANN C, POWELSKE C, MERGEN M, HERBST H, KOTSIS F, NITSCHKE R, KUEHN EW (2015). A cilia independent role of Ift88/polaris during cell migration. *PLoS One* 10: e0140378.
- BOIJE H, MACDONALD RB, HARRIS WA (2014). Reconciling competence and transcriptional hierarchies with stochasticity in retinal lineages. *Curr Opin Neurobiol* 27: 68–74.
- BOROVINA A, CIRUNA B (2013). IFT88 Plays a Cilia- and PCP-Independent Role in Controlling Oriented Cell Divisions during Vertebrate Embryonic Development. *Cell Rep* 5: 37–43.
- BOROVINA A, SUPERINA S, VOSKAS D, CIRUNA B (2010). Vangl2 directs the posterior tilting and asymmetric localization of motile primary cilia. *Nat Cell Biol* 12: 407–412.
- BRANCHEK T, BREMILLER R (1984). The development of photoreceptors in the zebrafish, *Brachydanio rerio*. I. Structure. *J Comp Neurol* 224: 107–115.
- CÁCERES A, YE B, DOTTI CG (2012). Neuronal polarity: demarcation, growth and commitment. *Curr Opin Cell Biol* 24: 547–553.
- CRESPO C, KNUST E (2018). Characterisation of maturation of photoreceptor cell subtypes during zebrafish retinal development. *Biol Open* 7: bio036632.
- ERDMANN B, KIRSCH F-P, RATHJEN FG, MORÉ MI (2003). N-cadherin is essential for retinal lamination in the zebrafish. *Dev Dyn* 226: 570–577.
- GÄRTNER A, FORNASIERO EF, DOTTI CG (2015). Cadherins as regulators of neuronal polarity. *Cell Adh Migr* 9: 175–182.
- HADJIVASILIOU Z, MOORE RE, MCINTOSH R, GALEA GL, CLARKE JDW, ALEXANDRE P (2019). Basal Protrusions Mediate Spatiotemporal Patterns of Spinal Neuron Differentiation. *Dev Cell* 49: 907–919.e10.
- HAPAK SM, ROTHLIN CV, GHOSH S (2018). PAR3–PAR6–atypical PKC polarity complex proteins in neuronal polarization. *Cell Mol Life Sci* 75: 2735–2761.
- HIGGINBOTHAM H, EOM T-YY, MARIANI LE, BACHLEDAA, HIRT J, GUKASSYAN V, CUSACK CL, LAI C, CASPARY T, ANTON ES (2012). Arl13b in Primary Cilia Regulates the Migration and Placement of Interneurons in the Developing Cerebral Cortex. *Dev Cell* 23: 925–938.
- HOON M, OKAWAH, DELLASANTINAL, WONG ROL (2014). Functional architecture of the retina: Development and disease. *Prog Retin Eye Res* 42: 44–84.
- KWAN KM, FUJIMOTO E, GRABHER C, MANGUM BD, HARDY ME, CAMPBELL DS, PARANT JM, YOST HJ, KANKI JP, CHIEN C-B (2007). The Tol2kit: a multisite gateway-based construction kit for Tol2 transposon transgenesis constructs. *Dev Dyn* 236: 3088–3089.

- LELE Z, FOLCHERT A, CONCHA M, RAUCH G-J, GEISLER R, ROSA F, WILSON SW, HAMMERSCHMIDT M, BALLY-CUIF L (2002). Parachute/N-Cadherin Is Required for Morphogenesis and Maintained Integrity of the Zebrafish Neural Tube. *Development* 129: 3281–3294.
- LEPANTO P, BADANO JL, ZOLESSI FR (2016). Neuron's little helper: the role of primary cilia in neurogenesis. *Neurogenesis* 3: 1–23.
- LEPANTO P, DAVISON C, CASANOVA G, BADANO JL, ZOLESSI FR (2016). Characterization of primary cilia during the differentiation of retinal ganglion cells in the zebrafish. *Neural Dev* 11: 10.
- MALICKI J (2012). Who drives the ciliary highway? *Bioarchitecture* 2: 111–117.
- MALICKI J, JO H, PUJIC Z (2003). Zebrafish N-cadherin, encoded by the glass onion locus, plays an essential role in retinal patterning. *Dev Biol* 259: 95–108.
- MASAI I, LELE Z, YAMAGUCHI M, KOMORI A, NAKATAA, NISHIWAKI Y, WADA H, TANAKAH, NOJIMAY, HAMMERSCHMIDT M, WILSON SW, OKAMOTO H (2003). N-cadherin mediates retinal lamination, maintenance of forebrain compartments and patterning of retinal neurites. *Development* 130: 2479–2494.
- OMORI Y, ZHAO C, SARAS A, MUKHOPADHYAY S, KIM W, FURUKAWA T, SENGUPTA P, VERAKSA A, MALICKI J (2008). Elipsa is an early determinant of ciliogenesis that links the IFT particle to membrane-associated small GTPase Rab8. *Nat Cell Biol* 10: 437–444.
- PRIETO D, APARICIO G, MORANDE PE, ZOLESSI FR (2014). A fast, low cost, and highly efficient fluorescent DNA labeling method using methyl green. *Histochem Cell Biol* 142: 335–345.
- PUJIC Z, MALICKI J (2004). Retinal pattern and the genetic basis of its formation in zebrafish. *Semin Cell Dev Biol* 15: 105–114.
- QUINN PM, PELLISSIER LP, WIJNHOLDS J (2017). The CRB1 Complex: Following the Trail of Crumbs to a Feasible Gene Therapy Strategy. *Front Neurosci* 11: 175.
- RANDLETT O, POGGI L, ZOLESSI FR, HARRIS WA (2011). The Oriented Emergence of Axons from Retinal Ganglion Cells Is Directed by Laminin Contact In Vivo. *Neuron* 70: 266–280.
- DE ROBERTIS E (1956). Morphogenesis of the retinal rods; an electron microscope study. *J Biophys Biochem Cytol* 2: 209–218.
- ROBU ME, LARSON JD, NASEVICIUS A, BEIRAGHI S, BRENNER C, FARBER SA, EKKER SC (2007). P53 Activation By Knockdown Technologies. *PLoS Genet* 3: e78.
- SHEN YC, RAYMOND PA (2004). Zebrafish cone-rod (crx) homeobox gene promotes retinogenesis. *Dev Biol* 269: 237–251.
- SUZUKI SC, BLECKERTA, WILLIAMS PR, TAKECHIM, KAWAMURAS, WONG ROL (2013). Cone photoreceptor types in zebrafish are generated by symmetric terminal divisions of dedicated precursors. *Proc Natl Acad Sci USA* 110: 15109–15114.
- TASCHNER M, WEBER K, MOURÃO A, VETTER M, AWASTHI M, STIEGLER M, BHOGARAJU S, LORENTZEN E (2016). Intraflagellar transport proteins 172, 80, 57, 54, 38, and 20 form a stable tubulin-binding IFT -B2 complex. *EMBO J* 35: 773–790.
- TSUJIKAWA M, MALICKI J (2004). Intraflagellar transport genes are essential for differentiation and survival of vertebrate sensory neurons. *Neuron* 42: 703–716.
- WEBER IP, RAMOS AP, STRZYZ PJ, LEUNG LC, YOUNG S, NORDEN C (2014). Mitotic position and morphology of committed precursor cells in the zebrafish retina adapt to architectural changes upon tissue maturation. *Cell Rep* 7: 386–397.
- WEI X, ZOU J, TAKECHI M, KAWAMURA S, LI L (2006). Nok plays an essential role in maintaining the integrity of the outer nuclear layer in the zebrafish retina. *Exp Eye Res* 83: 31–44.
- WHEWAY G, PARRY DA, JOHNSON CA (2014). The role of primary cilia in the development and disease of the retina. *Organogenesis* 10: 69–85.
- WONG GW, BAUDET M-L, NORDEN C, LEUNG L, HARRIS WA (2012). Slit1b-Robo3 signaling and N-cadherin regulate apical process retraction in developing retinal ganglion cells. *J Neurosci* 32: 223–228.
- ZOLESSI FR (2016). Vertebrate Neurogenesis: Cell Polarity. *eLS*: 1–14.
- ZOLESSI FR, POGGI L, WILKINSON CJ, CHIEN C-B, HARRIS WA (2006). Polarization and orientation of retinal ganglion cells in vivo. *Neural Dev* 1: 2.
- ZOU J, LATHROP KL, SUN M, WEI X (2008). Intact retinal pigment epithelium maintained by Nok is essential for retinal epithelial polarity and cellular patterning in zebrafish. *J Neurosci* 28: 13684–13695.
- ZOU J, WANG X, WEI X (2012). Crb apical polarity proteins maintain zebrafish retinal cone mosaics via intercellular binding of their extracellular domains. *Dev Cell* 22: 1261–1274.

Further Related Reading, published previously in the *Int. J. Dev. Biol.*

Mutation of *frizzled8a* delays neural retinal cell differentiation and results in microphthalmia in zebrafish

Xiao-Ning Cheng, Ming Shao and De-Li Shi

Int. J. Dev. Biol. (2018) 62: 285-291

<https://doi.org/10.1387/ijdb.170167ds>

The retinal pigmented epithelium – from basic developmental biology research to translational approaches

Benjamin Amram, Yamit Cohen-Tayar, Ahuvit David and Ruth Ashery-Padan

Int. J. Dev. Biol. (2017) 61: 225-234

<https://doi.org/10.1387/ijdb.160393ra>

Noggin 1 overexpression in retinal progenitors affects bipolar cell generation

Andrea Messina, Simone Bridi, Angela Bozza, Yuri Bozzi, Marie-Laure Baudet and Simona Casarosa

Int. J. Dev. Biol. (2016) 60: 151-157

<https://doi.org/10.1387/ijdb.150402am>

Alterations to retinal architecture prior to photoreceptor loss in a mouse model of retinitis pigmentosa

Sarah I. Roche, Alice C. Wyse-Jackson, Ashleigh M. Byrne, Ana M. Ruiz-Lopez and Thomas G. Cotter

Int. J. Dev. Biol. (2016) 60: 127-139

<https://doi.org/10.1387/ijdb.150400tc>

Development and programmed cell death in the mammalian eye

Elena Vecino and Arantxa Acera

Int. J. Dev. Biol. (2015) 59: 63-71

<https://doi.org/10.1387/ijdb.150070ev>

Ras-Related Nuclear Protein is required for late developmental stages of retinal cells in zebrafish eyes

Cheng-Yung Lin, Hsing-Yen Huang, Po-Nien Lu, Chien-Wei Lin, Kuang-Ming Lu and Huai-Jen Tsai

Int. J. Dev. Biol. (2015) 59: 435-442

<https://doi.org/10.1387/ijdb.150310ht>

Ocular forkhead transcription factors: seeing eye to eye

Holly E. Moose, Lisa E. Kelly, Srivamsi Nekkalapudi and Heithem M. El-Hodiri

Int. J. Dev. Biol. (2009) 53: 29-36

<https://doi.org/10.1387/ijdb.072505hm>

